ELSEVIER

Contents lists available at ScienceDirect

Psychiatry Research: Neuroimaging

journal homepage: www.elsevier.com/locate/psychresns



Hierarchical network disruptions in Schizophrenia: A multi-level fMRI study of functional connectivity*

V.S. Khorev ^{a,b}, S.A. Kurkin ^a, D. Stoyanov ^{c,d}, R. Paunova ^{c,d}, D. Najar ^{c,d}, S. Kandilarova ^{c,d}, A.E. Hramov ^a

- ^a Plekhanov Russian University of Economics, Research Institute of Applied Artificial Intelligence and Digital Solutions, Stremyanny per., 36, Moscow, 117997, Russia
- ^b Samara State Medical University, Gagarina str., 18, 443099, Samara, Russia
- ^c Medical University Plovdiv, Department of Psychiatry and Research Institute, Vassil Aprilov Blvd., 15A, 4002, Plovdiv, Bulgaria
- d Strategic Research and Innovation Program for the Development of MU-PLOVDIV-(SRIPD-MUP), European Union-NextGenerationEU, Vassil Aprilov Blvd., 15A, 4002, Plovdiv, Bulgaria

ARTICLE INFO

Keywords: fMRI Complex networks Schizophrenia Functional connectivity Neuroimaging biomarkers Cognitive impairment Multigraph

ABSTRACT

Background: We tested the hypothesis that Schizophrenia (SCZ) involves a systematic breakdown in brain network organization across different levels of graph-theoretical hierarchy.

Methods: Using resting-state fMRI from 43 SCZ patients and 63 matched healthy controls, we implemented an analytical multi-level framework. This integrated: global graph theory metrics to assess overall network topology; macronetwork metrics to measure functional specialization of large-scale systems; network-based statistics (NBS) to identify specific, altered pathways at the local level; a multigraph model to visualize hub reorganization between networks.

Results: We revealed a coherent pattern of multi-level dysfunction. Globally, SCZ networks showed increased local clustering and connection density, indicating a shift toward a less efficient, overly segregated architecture. At the macroscale, sensory and salience networks displayed elevated local connectivity, while higher-order cognitive networks (e.g., DMN, DAN) showed reduced specialization and increased cross-talk. Locally, NBS identified a core subnetwork of weakened connectivity within temporal-orbitofrontal-cingulate circuits. The multigraph model synthesized these findings, showing a widespread reduction in the integrative role of key cognitive hubs.

Conclusions: Our findings establish a model of SCZ as a disorder of disintegrated brain network hierarchy, where disruptions at the level of local circuits and functional specializations collectively lead to global topological inefficiency.

1. Introduction

The development of robust neuroimaging biomarkers for schizophrenia (SCZ) represents a critical need for improving diagnosis and personalized treatment of this complex psychiatric disorder (Varaprasad and Goel, 2025). Contemporary neuroscience conceptualizes SCZ as a disorder of brain network dysconnectivity, where disrupted integration and segregation of large-scale networks underlie its diverse symptomatology (Friston et al., 2016; Lynall et al., 2010; Więcławski W. Bielski et al., 2024). While resting-state functional MRI (rs-fMRI) has emerged

as a powerful tool for mapping these disruptions (Li et al., 2019; Voineskos et al., 2024; Zhang et al., 2024), a fundamental gap remains in understanding how alterations at different hierarchical scales – from global network architecture to local circuit dysfunction – collectively contribute to the pathophysiology of SCZ.

Traditional fMRI studies of SCZ have predominantly focused on either isolated regional abnormalities or pairwise connectivity between predefined networks (Sheffield et al., 2015; Repovs et al., 2011; Chatterjee and Hilal, 2024). This approach has identified key alterations

E-mail addresses: khorevvs@gmail.com (V.S. Khorev), kurkinsa@gmail.com (S.A. Kurkin), drozdstoy.stoyanov@mu-plovdiv.bg (D. Stoyanov), Rositsa.Paunova@mu-plovdiv.bg (R. Paunova), Diyana.Nazhar@mu-plovdiv.bg (D. Najar), Sevdalina.Kandilarova@mu-plovdiv.bg (S. Kandilarova), hramovae@gmail.com (A.E. Hramov).

https://doi.org/10.1016/j.pscychresns. 2025.112078

^{*} Correspondence to: Samara State Medical University, Gagarina str., 18, 443099, Samara, Russia.

^{**} Corresponding author.

in networks such as the default mode network (DMN) (Buckner, 2013; Menon, 2023; Whitfield-Gabrieli and Ford, 2012; Zhou et al., 2016), salience network (SN) (Uddin, 2014; Huang et al., 2022), and frontoparietal network (Li et al., 2019; Liang et al., 2021). However, these investigations often fail to capture the multi-level nature of network disruption in SCZ, where global topology may appear preserved while critical subsystem interactions become profoundly impaired (Li et al., 2019; Kurkin et al., 2025). Moreover, existing frameworks struggle to explain how localized disruptions in circuits like the orbitofrontal cortex or thalamocortical pathways propagate to produce system-wide dysfunction (Dong et al., 2018).

Our study addresses these gaps through three key innovations. First, we integrate analyses across hierarchical levels – global (whole-brain topology), macro (large-scale network interactions), and local (individual node connectivity) – to provide a unified view of SCZ-related disruptions. In this context, we define hierarchical network dysfunction as the pathological disruption of the brain's nested organization, where abnormalities at one level (e.g., local circuit disconnection) systematically propagate to alter functional dynamics at higher levels (e.g., macronetwork specialization and global integration). Second, we use a modified participation coefficient that specifically quantifies imbalances in network integration versus segregation, overcoming limitations of conventional metrics in overlapping functional systems. Third, we employ a multigraph model to visualize how focal disruptions affect the entire network architecture, bridging the gap between localized connectivity changes and their global functional consequences.

2. Materials and methods

2.1. Subjects

The study involved 106 participants: 43 patients with schizophrenia (Sz group) and 63 healthy control subjects (HC group). Sociodemographic group characteristics do not differ statistically as presented in Table 1. All participants underwent a diagnostic clinical interview conducted by a physician and were screened for comorbidities, using MINI (Sheehan et al., 1998). Schizophrenia symptoms were evaluated using the Positive and Negative Symptom Scale (PANSS) (Kay et al., 1987). There has been estimated the total score, as well as the scores on positive (P), negative (N), and general psychopathology (G) scales. Positive scale captures productive symptoms, including assessment of verbal-acoustic hallucinations (item P3), whereas the negative scale is supposed to capture the deficit symptoms. Based on the diagnostic assessment, the patients fulfilled the DSM-V criteria for schizophrenia. The leading clinical inclusion criteria were set as total PANSS score above 60, and positive scale score above 4, with an additional criterion of P3> 3 (Table 1). The assessment of P3 (manifestation of auditory verbal hallucinations) was performed under the rationale of another research project (Zaykova et al., 2025).

All patients received stable dose atypical antipsychostics maintenance treatment. Healthy volunteers were recruited from the local community. Exclusion criteria for healthy participants comprised neurological disorders, psychiatric illnesses, and a history of traumatic brain injury. The Ethics Committee of Medical University of Plovdiv approved the study (Protocol No. 1/11.01.2024). The research protocol complied with the 1964 Helsinki Declaration and its subsequent amendments. All participants provided voluntary written informed consent, allowing for the publication of any potentially identifiable images or data included in this manuscript.

2.2. Data acquisition

The MR scanning procedure was performed on a 3T MRI system (GE Discovery 750w). The protocol included a high-resolution structural scan (Sag 3D T1) with slice thickness of 1 mm, matrix 256 \times 256, TR (relaxation time) 7.2 s, TE (echo time) 2.3 s, and flip angle 12°, FOV 24, resting-state functional scan — with slice thickness 3 mm, matrix 64 \times 64, repetition time — 2000 ms, echo time — 30 ms, flip angle 90°, 192 volumes (Stoyanov et al., 2020).

 Table 1

 Socio-demographic and clinical characteristics.

Characteristic	Sz $(n = 43)$	HC $(n = 63)$	p
Age (Mean±SD)	35.4 ± 12.4	36.0 ± 12.5	0.771^{a}
Sex (M/F)	26/17	31/32	0.253^{b}
PANSS total score (mean±SD)	71 ± 12	-	-
PANSS-P score (mean±SD)	20 ± 3	-	-
PANSS P3 score (mean±SD)	5.1 ± 0.62	1.0 ± 0.0	0.000*a
Illness duration, days (mean±SD)	138 ± 85	-	-

SD – Standard Deviation, ^a Student's t-test, ${}^{b}\chi^{2}$ – test, * – p < 0.05.

2.3. Preprocessing

The whole pipeline of the study is schematically represented in Fig. 1. The functional images were pre-processed with SPM 12 software (SPM, 2024) in a typical way (see Sec. 2.1.3 in Ref. Pitsik et al. (2023) for the details). Standard preprocessing procedures were employed, including motion correction, co-registration with high-resolution T1, and normalization to the Montreal Neurological Institute's standard space (Khorev et al., 2025; Kurkin et al., 2024; Andreev et al., 2023). We omitted slice timing correction because the temporal discrepancy between slices was negligible relative to the hemodynamic response given the 2000 ms TR and our experimental design. Filtering is effectively performed during the subsequent detrending step. As a result, we obtained voxel-level blood-oxygen-level-dependent (BOLD) signals.

Using the AAL3 anatomical atlas (Rolls et al., 2020), we divided the brain into 165 distinct regions. To measure functional connectivity, we first averaged the BOLD time series within each region and treated each region as a network node to construct a connectivity matrix. This parcellation step also serves as a smoothing procedure. After detrending these averaged time series, we computed pairwise Pearson correlation coefficients between all nodes. Only connections with p < 0.05 were kept (Pisarchik et al., 2023). This resulting connectivity matrix captures the functional brain network, reflecting the coupling strength between different brain regions based on their correlated BOLD signals (Fig. 1, panel II). The values in the matrices were taken modulo for the calculation of network measures.

2.4. Network analysis

Our approach considers several levels of network interaction:

- Global level: Interactions between macronetworks large-scale networks (LSNs) – treated as single units or macronodes (Yang et al., 2016; Wang et al., 2020).
- Macro level: Interactions between macronetworks, accounting for both (i) intra-macronetwork node interactions and (ii) intermacronetwork node connections (Kelly and Castellanos, 2014; Hardikar et al., 2024).
- Local level: Interactions between individual nodes within the original network.

For global level analysis, we considered 15 macronetworks (see Table 2) from Zwir et al. (2023), encompassing all major LSNs. The global correlation matrix (15 \times 15) was constructed using pairwise Pearson correlations between macronetworks, derived from their mean BOLD signals (averaged across constituent nodes — see Fig. 1, panels II and III).

2.5. Network characteristics

2.5.1. Network measures

We computed a set of network measures for both the global network and each local macronetwork (Fig. 1, panel IV):

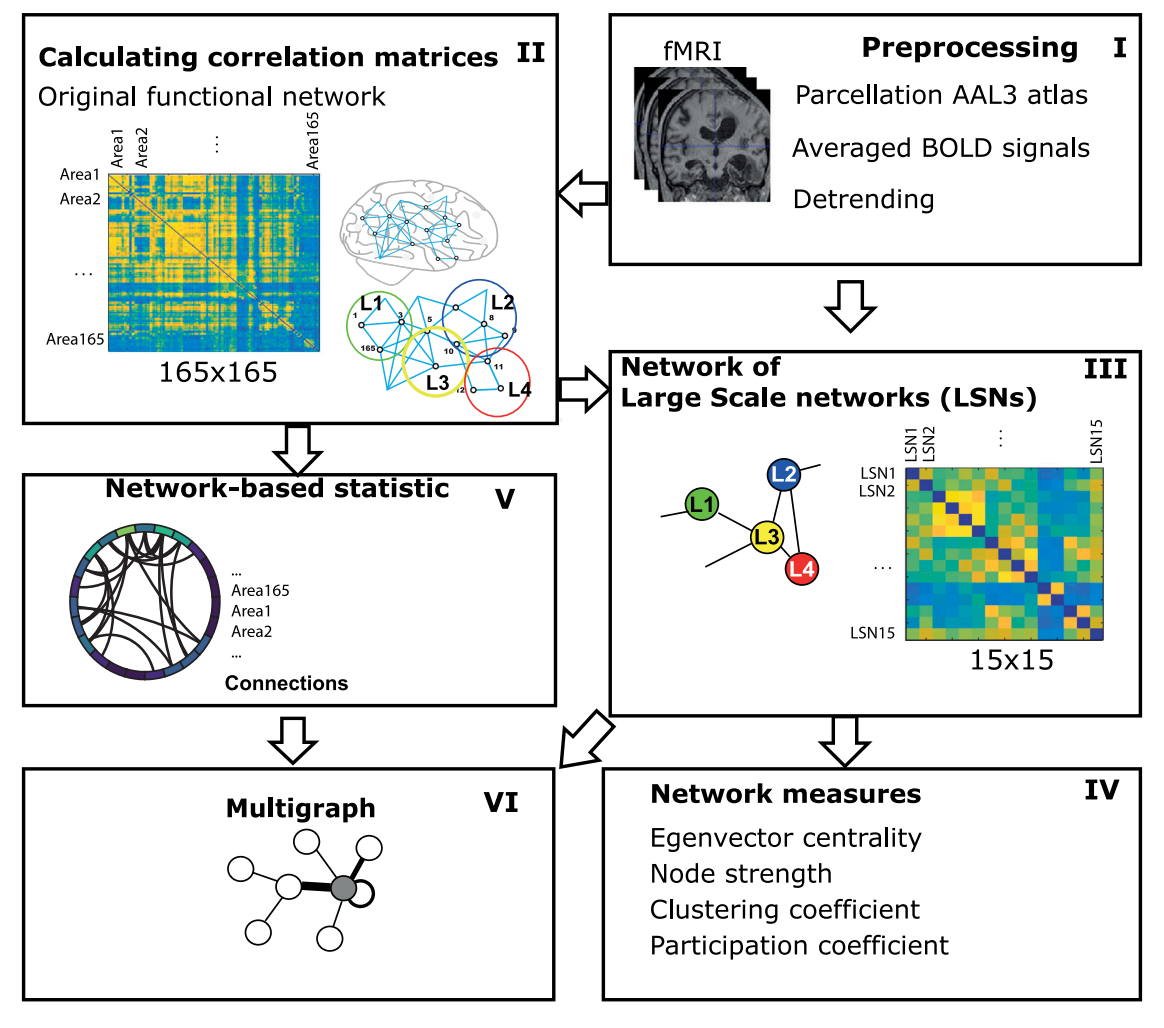


Fig. 1. The schematic pipeline of the study.

- Clustering Coefficient: Measures local network cohesiveness by quantifying the tendency of nodes to form densely interconnected clusters, reflecting the density of connections among a node's direct neighbors (Costantini and Perugini, 2014; Khorev et al., 2024).
- Node Strength: Generalizes degree centrality to weighted networks by summing the weights of all edges connected to a node, representing its total interaction strength within the network (Rubinov and Sporns, 2011).
- Global Efficiency: Evaluates the network's information integration capacity by computing the average inverse shortest path length between all node pairs, with higher values indicating more efficient parallel information transfer (Onnela et al., 2005).
- Eigenvector Centrality: Assesses a node's influence based on its connections to other highly central nodes, derived from the principal eigenvector of the network's adjacency matrix. High centrality indicates a strategically important position in the network (Newman, 2008).

2.5.2. Modified participation coefficient

We used a modified participation coefficient (PC) tailored for singlenetwork communities (Kurkin et al., 2025), defined as:

$$P_i = 1 - \left(\frac{w_{is}}{w_i}\right)^2,\tag{1}$$

where P_i represents the modified PC for node i, w_{is} denotes the total connection weight between node i and other nodes within its community, and w_i is the node i's total strength (sum of all connection

weights, intra- and inter-community). This metric quantifies a node's position relative to its community, where $P_i \rightarrow 1$ indicate connector nodes with predominantly external connections (gateway nodes), while $P_i \rightarrow 0$ reflects a core nodes with primarily internal connections.

To assess whole-community properties, we computed the community-averaged PC:

$$\langle P \rangle_k = \frac{1}{|\mathcal{C}_k|} \sum_{i \in \mathcal{C}_k} P_i,\tag{2}$$

where \mathcal{C}_k are nodes in community k and $|\mathcal{C}_k|$ is the community size. The averaged PC provides insights into community organization: low values ($\langle P \rangle \to 0$) indicate strongly segregated communities with predominantly internal connections, while high values ($\langle P \rangle \to 1$) suggest communities heavily dependent on external connections. A balanced community with equal internal and external connectivity would yield $\langle P \rangle = 0.75$.

For macro-level analysis, we treated the 15 predefined LSNs (Table 2) as distinct communities (k = 1, ..., 15) and computed their P values. This adaptation resolves two key limitations of the standard PC Guimera and Nunes Amaral (2005): (1) ambiguity in overlapping communities (typically for LSNs), and (2) robust quantification of integrative (external) vs. segregative (internal) properties.

Hereafter, we refer to this modified metric simply as the participation coefficient (PC).

2.5.3. Statistical analysis

For local-level network comparisons, we applied the network-based statistic (NBS) method (Zalesky et al., 2010) to identify significantly

Table 2
Considered large-scale networks (LSNs)/macronetworks (Zwir et al., 2023).

LSN	Abbreviation	Main constituent brain regions (nodes)
Auditory Network	AN	Heschl's gyrus, Bilateral Superior Temporal gyri, Posterior Insular Cortex, et al.
Cingulo-Opercular Network	CON	Anterior Insula/Operculum, Dorsal Anterior Cingulate Cortex, Thalamus, et al.
Context Network	Context	Parahippocampal Cortex, Retrosplenial Cortex
Default Mode Network	DMN	Posterior Cingulate Cortex, Precuneus, Medial Prefrontal Cortex, Angular Gyrus
Dorsal Attention Network	DAN	Visual Motion Area, Frontal Eye Fields, Superior Parietal Lobule Intraparietal Sulcus, Ventral Premotor Cortex
Perception Network	perN	Lateral Orbitofrontal, Ventromedial Temporal, Temporal Pole, Subgenual Anterior Cingulate Cortices, Fusiform Gyrus, Rostral Superior Temporal Sulcus, Ventrolateral Amygdala
Somatomotor Network	SMN	S1, M1, Supplementary Motor Area (SMA), Thalamus
Striatum	Striatum	Caudate, Putamen, Ventral Striatum
Thalamus	Th	Thalamic Nuclei, Subcortical Regions
Ventral Attention Network	VAN	Bilateral Ventrolateral Prefrontal Cortex, Bilateral Temporal-Parietal Junction
Visual Network	Visual	Middle Temporal Visual Association Area at the Temporal-Occipital Junction
Fronto-Parietal Network	FPN	Intraparietal Sulcus, Ventral Inferior Temporal Lobe, Lateral Prefrontal Cortex
Salience Network	SN	Limbic and Prefrontal Regions, Amygdala, Anterior Insula, Dorsal Anterior Cingulate Cortex, Ventral Striatum
Amygdala Network	Amygdala	Amygdala, Precuneus, Nucleus Accumbens
Entorhinal-Hippocampal Network	EHN	Olfactory Bulb, Hippocampus, Parahippocampal area, Temopral lobe

altered subnetworks in the complete 165×165 connectivity matrix between groups (Fig. 1, panel V). Instead of controlling the error rate at the level of individual edges in a connectivity matrix – which can be excessively conservative when large numbers of edges are tested simultaneously – NBS adopts a cluster-based approach. The analysis was performed with 50,000 permutations using a primary threshold of t=3.1 (p=0.05), providing robust control for multiple comparisons while maintaining sensitivity to detect connected patterns of altered connectivity.

At the global and macro levels, we compared network measures between groups using the two-sided Mann–Whitney U test. The test was applied to node-averaged values of each network metric to evaluate systematic between-group differences in network topology.

The PANSS scales were correlated post-hoc with the network measures using Pearson correlation.

IWe implemented the Bonferroni correction to account for multiple comparisons across macronetworks. In the correlation analysis, we applied the Benjamini–Hochberg procedure to control the false discovery

rate. We applied these corrections separately for each type of network measure (e.g., clustering coefficient and global efficiency) across all 15 macronetworks to ensure rigorous control of false positives.

2.6. Multigraph representation of altered network interactions

To effectively visualize the disrupted patterns of communication between large-scale networks (LSNs) in schizophrenia, we developed a multigraph model (Kurkin et al., 2025). This model was constructed by incorporating statistically significant connections that differed between patient and control groups. In our visual representation, the thickness of an edge between any two LSNs directly corresponds to the total number of disrupted connections they share, providing an intuitive, quantitative assessment of how severely their interaction is altered. A key strength of this model is its ability to integrate information across multiple scales, combining macro-level changes in network participation coefficient with local-level disruptions in connectivity. This integrated method effectively illustrates how localized, individual connection failures propagate upward to produce significant alterations in

Table 3Between-group comparisons of the global-level network measures. Statistical tests were performed for the network of large-scale networks (LSNs).

Measure	$SZ M \pm SD$	HC M \pm SD	d Sz>HC	u Sz>HC	p
Global efficiency	7.43 ± 15.63	3.94 ± 3.17	0.31	1.9303	0.0536
Eigenvector centrality	0.26 ± 0.00	0.26 ± 0.00	0.02	0.3667	0.7138
Node strength	9.07 ± 1.88	8.29 ± 1.26	0.49	2.4193	0.0156*
Clustering coefficient	0.70 ± 0.15	0.64 ± 0.10	0.46	2.3807	0.0173*

^{*} indicates significant changes; d is Cohen's d.

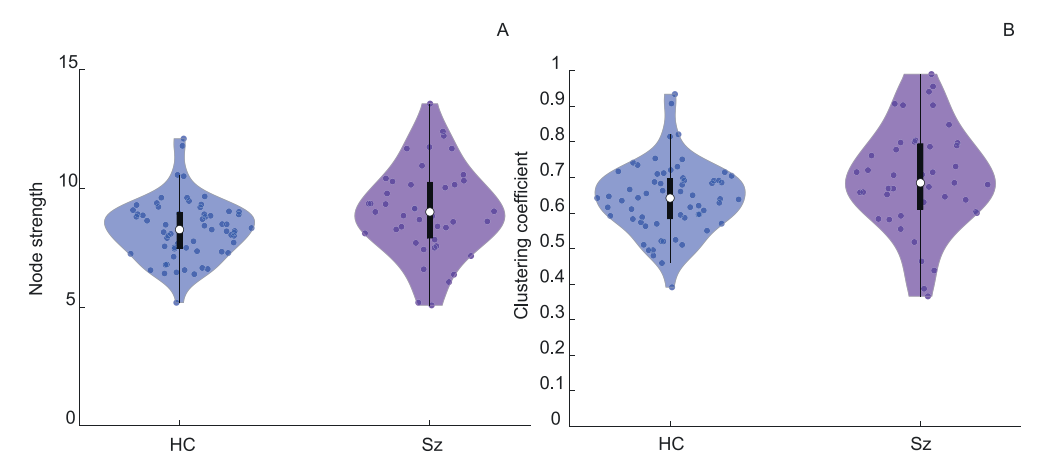


Fig. 2. Difference in distributions of network measures on global level between groups (A) Node strength, (B) Clustering coefficient.

the integration-segregation balance at the level of LSNs, which in turn manifest as changes in the brain's overall network organization.

3. Results

Significant between-group differences emerged at the global level (network of LSNs) for node strength and clustering coefficient (Table 3 and Fig. 2), indicating altered functional connectivity architecture in schizophrenia. Patients exhibited elevated node strength, reflecting increased overall connectivity between LSNs. Paradoxically, this hyperconnectivity co-occurred with higher clustering coefficient, suggesting a shift toward fragmented, locally dense clusters of LSNs.

At the macroscale level (Tables 4–6), these group differences persist across all measures, but with important regional specificity. Notably, significant differences in eigenvector centrality are confined to the auditory network, implying that this network may play a particularly central or influential role in the altered connectivity patterns seen in schizophrenia. For node strength and clustering coefficient, the differences are consistently observed in six out of the fifteen LSNs: Auditory, Cingulo-Opercular, Somatomotor, Thalamus, Salience, and Entorhinal-Hippocampal networks. This suggests that the disruptions in network local hyperconnectivity and clustering are not uniformly distributed across the brain, but are instead concentrated within specific functional systems.

Analysis of the macronetwork-averaged PC revealed significant between-group differences in several LSNs, as shown in Table 7. Specifically, significant alterations in PC were observed in 6 out of 15 LSNs: Context, Default Mode, Dorsal Attention, Perception, Entorhinal-Hippocampal networks, and most notably, the Visual network. Importantly, the set of LSNs showing altered PC is largely distinct from those identified by differences in node strength or clustering coefficient, with the exception of the Entorhinal-Hippocampal network.

The participation coefficient is a measure that reflects the extent to which nodes within a network are connected to nodes in other networks, thus capturing the balance between within-network (intra-LSN) and between-network (inter-LSN) connectivity. The observed increases in PC among affected LSNs indicate that nodes within these networks

Table 4Between-group differences in eigenvector centrality (EC) at the macro level across predefined large-scale networks (LSNs).

LSN	$SZ M \pm SD$	HC M \pm SD	d Sz>HC	u Sz>HC	p
AN	0.35 ± 0.01	0.34 ± 0.01	0.38	2,7603	0,0058*
CON	0.13 ± 0.01	0.13 ± 0.01	0.27	1,4348	0,1513
Context	0.38 ± 0.03	0.38 ± 0.02	-0.02	0,2059	0,8369
DMN	0.39 ± 0.02	0.40 ± 0.01	-0.24	-0,4890	0,6248
DAN	0.34 ± 0.02	0.34 ± 0.02	0.08	0,4182	0,6758
perN	0.23 ± 0.01	0.23 ± 0.01	-0.01	0,8751	0,3815
SMN	0.15 ± 0.01	0.15 ± 0.01	0.33	1,8852	0,0594
Striatum	0.38 ± 0.03	0.38 ± 0.02	0.07	1,3640	0,1726
Th	0.14 ± 0.01	0.14 ± 0.01	0.28	1,2482	0,2119
VAN	0.30 ± 0.02	0.30 ± 0.02	-0.03	0,2831	0,7771
Visual	0.39 ± 0.02	0.39 ± 0.02	-0.13	-0,2381	0,8118
FPN	0.34 ± 0.01	0.34 ± 0.02	0.12	1,1517	0,2494
SN	0.23 ± 0.01	0.23 ± 0.01	0.14	1,7951	0,0726
Amygdala	0.37 ± 0.04	0.35 ± 0.05	0.29	1,5120	0,1305
EHN	$0.34~\pm~0.02$	$0.34~\pm~0.01$	-0.12	0,9651	0,3345

^{*} indicates significant changes; d is Cohen's d; no comparisons survive the Bonferroni correction.

tend to have a greater proportion of outward-directed connections to other LSNs than inward-directed connections within their own network in schizophrenia. This result is consistent with the effect obtained at the global level for node strength (Table 3).

At the local level, the NBS results reveal (see Fig. 3) 15 significantly different local connections between 17 nodes in the original 165×165 network in the HC > Sz direction. The node with the highest degree of alternations is Temporal Inf L, while the nodes with relatively high degrees are Cingulate Mid R, Occipital Mid R, and OFCpost L and R. Notably, Temporal Inf L shows broadly reduced connections to the motor (Precentral R), limbic (OFCant L and Cingulate Mid L), and sensorimotor (Paracentral Lobule R) regions. Meanwhile, the OFCpost L/R exhibit reduced integration of visual (Occipital Mid R) and thalamic inputs (Thal PuA R), as well as cingulate and parietal feedback (Cingulate Mid R).

The multigraph visualization (Fig. 4) provides further insight into these connectivity alterations from the perspective of the NBS method.

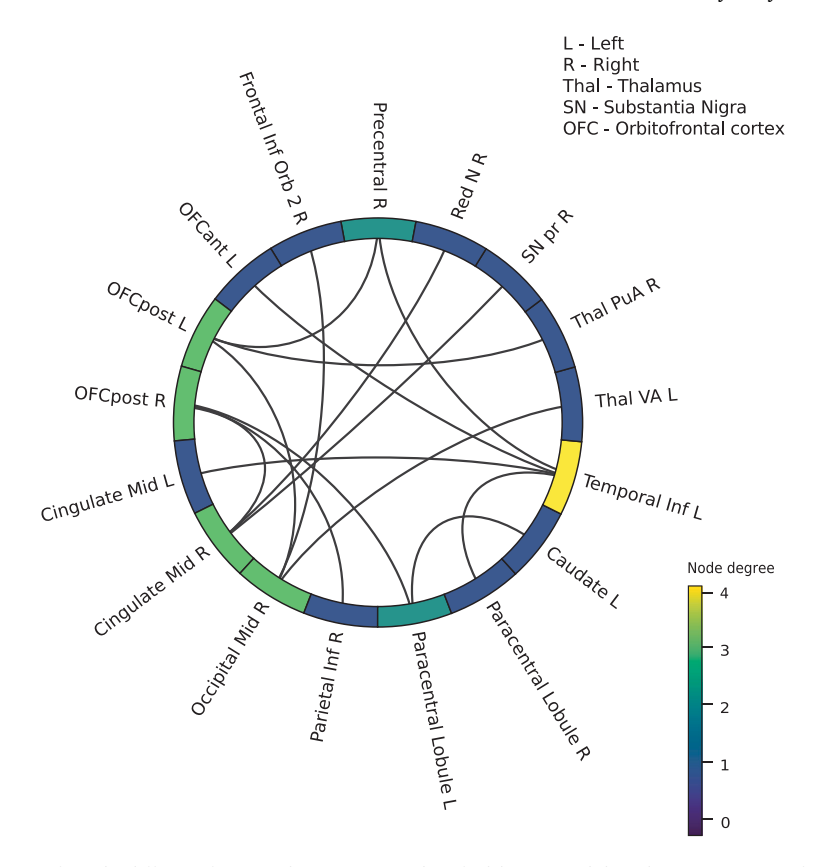


Fig. 3. Connectogram displaying significantly different functional connections identified by network-based statistics (NBS) for HC > Sz. Node color represents the degree of connectivity alterations, scaled by the number of significantly different connections per node.

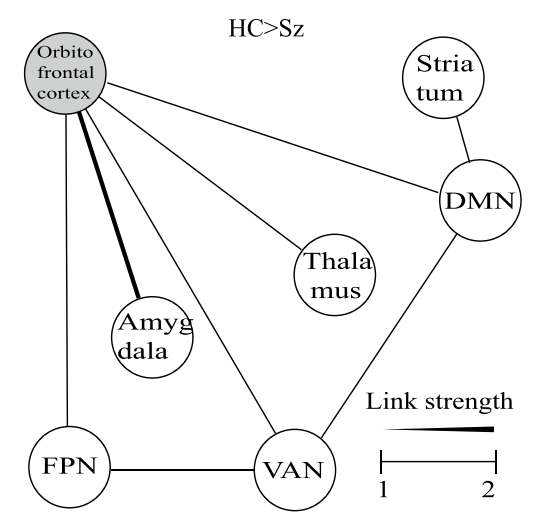
Table 5Between-group differences in node strength (NS) at the macro level across predefined large-scale networks (LSNs).

LSN	SZ M ± SD	HC M ± SD	d Sz>HC	u Sz>HC	p
AN	3.40 ± 1.17	2.83 ± 0.95	0.53	2,8568	0,0043*
CON	7.86 ± 6.22	5.02 ± 3.57	0.56	2,6638	0,0077*
Context	1.84 ± 0.74	1.63 ± 0.53	0.34	1,3769	0,1685
DMN	2.33 ± 0.79	2.29 ± 0.72	0.06	0,2702	0,7870
DAN	2.92 ± 1.11	2.93 ± 0.95	-0.00	-0,3410	0,7331
perN	5.56 ± 2.29	4.93 ± 1.79	0.30	1,8724	0,0612
SMN	5.98 ± 4.67	4.11 ± 2.82	0.48	2,1876	0,0287*
Striatum	1.89 ± 1.12	1.44 ± 0.65	0.49	1,6214	0,1049
Th	6.04 ± 5.09	3.75 ± 2.79	0.56	2,7217	0,0065*
VAN	3.32 ± 1.60	2.72 ± 1.01	0.44	1,5571	0,1195
Visual	2.08 ± 0.83	1.91 ± 0.73	0.22	1,0037	0,3155
FPN	3.13 ± 1.36	2.73 ± 1.05	0.33	1,2482	0,2119
SN	5.31 ± 2.58	4.21 ± 1.58	0.52	2,5865	0,0097*
Amygdala	1.47 ± 0.81	1.18 ± 0.48	0.43	1,5442	0,1225
EHN	3.29 ± 1.39	$2.70~\pm~0.98$	0.49	2,2906	0,0220*

 $^{^{\}ast}$ indicates significant changes; d is Cohen's d; no comparisons survive the Bonferroni correction.

One striking pattern is the predominance of increased connections between LSNs in the control group, particularly involving central hubs such as the DMN, Ventral Attention Network (VAN), Fronto-Parietal Network (FPN), as well as nodes in the orbitofrontal cortex that are not assigned to any specific LSN. Nodes of the orbitofrontal cortex participate in the communication with the thalamic nodes and amygdala, while Striatum only has one connection with DMN.

We examined correlations between PANSS scores and network measures to identify clinically relevant associations. While no significant correlations were observed at the global level, several emerged at the macroscale (Tables 8–11 in Appendix). However, these correlations did not survive correction for multiple comparisons. These results and limitations are discussed further in the respective sections.



DMN - Default Mode Network

FPN - Frontoparietal Network

VAN - Visual Attention Network

Fig. 4. The multigraph combining information about LSNs and NBS-derived connections that are significantly different for the HC > Sz direction.

4. Discussion

Most of our findings aligned with previous literature, reinforcing established models of network dysconnectivity in SCZ. However, some discrepancies emerged, highlighting potential directions for future research. Notably, significant group differences were observed in node strength and clustering coefficient at the global level, with SCZ

Table 6Between-group differences in clustering coefficient (CC) at the macro level across predefined large-scale networks (LSNs).

LSN	$SZ M \pm SD$	HC M \pm SD	d Sz>HC	u Sz>HC	p	p-bc
AN	0.37 ± 0.14	0.30 ± 0.13	0.57	3,1142	0,0018*	0,027*
CON	0.13 ± 0.15	0.07 ± 0.08	0.54	2,7796	0,0054*	0,081
Context	0.22 ± 0.13	0.19 ± 0.10	0.29	1,1002	0,2712	1
DMN	0.32 ± 0.14	0.31 ± 0.13	0.03	0,0579	0,9538	1
DAN	0.29 ± 0.15	0.29 ± 0.13	0.00	-0,4182	0,6758	1
perN	0.28 ± 0.15	0.24 ± 0.12	0.28	1,7115	0,0870	1
SMN	0.12 ± 0.14	0.07 ± 0.08	0.47	2,3292	0,0198*	0,297
Striatum	0.25 ± 0.19	0.17 ± 0.11	0.51	1,6407	0,1009	1
Th	0.12 ± 0.14	0.06 ± 0.07	0.53	2,7731	0,0056*	0.084
VAN	0.26 ± 0.17	0.20 ± 0.11	0.43	1,4027	0,1607	1
Visual	0.27 ± 0.14	0.24 ± 0.13	0.17	0,7850	0,4325	1
FPN	0.33 ± 0.18	0.28 ± 0.14	0.31	1,0745	0,2826	1
SN	0.26 ± 0.16	0.19 ± 0.10	0.51	2,4000	0,0164*	0.246
Amygdala	0.16 ± 0.13	0.12 ± 0.08	0.43	1,5120	0,1305	1
EHN	0.35 ± 0.18	0.28 ± 0.13	0.46	1,9753	0,0482*	0.723

^{*} indicates significant changes; p-bc is Bonferroni-corrected p-value; d is Cohen's d.

Table 7Between-group differences in participation coefficient (PC) at the macro level across predefined large-scale networks (LSNs).

LSN	$SZ M \pm SD$	HC M \pm SD	d Sz>HC	u Sz>HC	p	p-bc
Auditory	0.9933 ± 0.0028	0.9928 ± 0.0027	0.1549	1,0616	0,2884	1
CingularOper	0.9230 ± 0.0118	0.9214 ± 0.0182	0.1098	0,1802	0,8570	1
Context	0.9968 ± 0.0016	0.9958 ± 0.0024	0.4859	2,1619	0,0306*	0.459
DMN Zwir	0.9946 ± 0.0032	0.9931 ± 0.0038	0.4156	2,2713	0,0231*	0.3465
DAN Zwir	0.9927 ± 0.0027	0.9912 ± 0.0035	0.4826	2,7345	0,0062*	0.093
perN	0.9784 ± 0.0068	0.9741 ± 0.0087	0.5568	2,4321	0,0150*	0.2550
Somatomotor	0.9467 ± 0.0111	0.9421 ± 0.0181	0.3084	1,0745	0,2826	1
Striatum	0.9974 ± 0.0011	0.9972 ± 0.0012	0.1797	0,8815	0,3781	1
Thalamus	0.9422 ± 0.0104	0.9392 ± 0.0184	0.2004	0,2960	0,7673	1
VAN	0.9918 ± 0.0026	0.9914 ± 0.0024	0.1388	0,8171	0,4138	1
Visual	0.9974 ± 0.0015	0.9965 ± 0.0020	0.4707	3,0498	0,0023*	0.0345*
FPN	0.9934 ± 0.0022	0.9935 ± 0.0020	-0.0240	0,1287	0,8976	1
SN	0.9801 ± 0.0053	0.9784 ± 0.0057	0.2958	1,6793	0,0931	1
Amygdala	0.9982 ± 0.0008	0.9980 ± 0.0011	0.1955	0,5791	0,5625	1
EHN	0.9938 ± 0.0022	0.9929 ± 0.0025	0.4073	2,1490	0,0316*	0.474

 $^{^{\}ast}$ indicates significant changes; p-bc is Bonferroni-corrected p-value; d is Cohen's d.

demonstrating higher values than HC. These findings suggest that, at the whole-brain scale, schizophrenia is associated with increased local network integration, reflecting a brain that is more densely connected but potentially less segregated. In other words, the networks in patients show signs of being over-connected in an inefficient manner — exhibiting higher overall connectivity alongside excessive local clustering. Such a configuration indicates a breakdown in the brain's critical balance between integration and segregation. This disrupted network organization is consistent with the broader concept of dysconnectivity in psychosis, where altered connectivity patterns contribute to cognitive and functional impairments (Skåtun et al., 2016; Lynall et al., 2010).

Based on these observations, we examined the relationship between symptom severity and network organization characteristics. No significant correlations were observed between global measures and PANSS scores, suggesting that symptoms do not uniformly affect wholebrain integration or segregation. Instead, negative symptoms, as well as positive symptoms to a lesser extent, were consistently linked to reduced hubness and local clustering in the CON, SMN, thalamus, VAN, and Context Network. This pattern indicates hypoconnectivity and weakened functional specialization across control, sensorimotor, attentional, and associative hubs, reflecting both diminished influence within the network and local disorganization.

In our analyses, the correlation between the Context Network and total PANSS scores is particularly noteworthy. The Context Network, which primarily includes the parahippocampal cortex and the retrosplenial cortex, has been strongly implicated in human spatial navigation, a function closely tied to higher-order cognitive processes (Epstein,

2008). From a clinical perspective, this finding is intriguing because SCZ is characterized not only by perceptual disturbances but also by deficits in reality monitoring and cognitive insight. Previous work has linked abnormalities in these medial temporal and retrosplenial regions to impaired reality processing and altered integration of contextual information, which may contribute to difficulties in distinguishing internal from external experiences (Lee et al., 2015). Accordingly, the observed association between PANSS severity and Context Network disruptions may reflect a neural substrate underlying both cognitive and perceptual alterations in SCZ. In this framework, higher symptom burden could exacerbate the breakdown of contextual representations, impairing the ability to organize and interpret environmental and internal cues coherently. These findings suggest that altered connectivity within the Context Network may serve as a mechanistic link between cognitive dysfunction, perceptual anomalies, and the clinical expression of symptom severity in schizophrenia. Thus, the revealed nuanced patterns suggest that SCZ disruptions are not uniformly global, but rather manifest more strongly within specific functional systems, affecting both hub influence and local network integrity.

Extending this analysis to macronetwork measures, patients with SCZ exhibited altered eigenvector centrality and increased node strength within the Auditory Network (AN). Increases in node strength were also observed in the Cingulo-Opercular Network (CON), Thalamus (Th), Somatomotor Network (SMN), Salience Network (SN), and Entorhinal-Hippocampal Network (EHN). Similarly, clustering coefficients were higher in the AN, CON, SMN, Th, SN, and EHN. Significant group differences in participation coefficient emerged across several networks, including the Default Mode Network (DMN), Dorsal Attention

Network (DAN), Context Network, Perception Network (perN), Visual Network (VN), and EHN. The involvement of both sensory and control-related networks points to widespread disruptions that may underlie the heterogeneous symptomatology observed in SCZ. In summary, the results on network measures at the macro level suggest two main findings:

- Local Disorganization: In sensory and salience-related networks (Auditory, Salience, etc.), the schizophrenia-related disruptions include high local density and fragmentation (high node strength and clustering), which suggests inefficient processing within these systems.
- Boundary Disintegration: In higher-order cognitive networks (Default Mode Network, Dorsal Attention, Perception, and Visual), the main disruption is a loss of functional specialization. These networks form relatively excessive connections outside their own boundaries, resulting in high PC and blurring their distinct roles. This causes pathological "cross-talk" between systems that should be more segregated, such as those responsible for internal thoughts and external attention.

This EHN network is the only one affected in both analyses. This makes sense as the hippocampus participates both in processing information locally (memory consolidation) and linking that information to widespread cortical networks for context (memory retrieval). The finding suggests it is failing at both its local and global roles, making it a critical hub for pathology.

Network-Based statistics (NBS) also revealed reduced inter-regional connectivity in patients compared to controls with no region showing increased connectivity in SCZ. This pattern can imply lowered integrative hub function, which would result in network-level "disconnection" consistent with the classic "dysconnectivity hypothesis" of SCZ (Friston et al., 2016). These findings highlight that schizophrenia is associated with both global and regionally specific alterations in brain network organization. The increased node strength and clustering at the global level, together with the targeted disruptions in particular LSNs, point to a complex reorganization of network topology that may underlie the cognitive and clinical features of the disorder. The observed changes in the participation coefficient suggest a shift toward greater global integration of networks and reduced modularity, which may reflect a breakdown in the functional specialization of these LSNs.

Building on these network findings, it is pertinent to consider established structural alterations that may underpin these functional changes, such as those observed in the orbitofrontal cortex (OFC). Studies consistently report reduced gray matter volume and cortical thickness of the OFC in individuals with SCZ compared to healthy controls. For example, diminished medial orbitofrontal cortex (MOFC) thickness is significantly associated with greater negative symptom severity, such as apathy and anhedonia, supporting the notion that OFC structural alterations underpin some negative symptoms (Nakamura et al., 2007; Walton et al., 2017; Dong et al., 2025). Besides that, altered sulcogyral patterns (the folding structure of the OFC) were also found in SCZ, suggesting prenatal neurodevelopmental disruptions may contribute to the disorder's vulnerability, with distinct alterations especially evident in female patients (Isomura et al., 2017). Exaggerated gyrification (folding of the cortex) of the OFC was also found - particularly in chronic auditory verbal hallucinators - showing abnormal wiring or connectivity in this subgroup (Núñez et al., 2024). There is some evidence for smaller OFC subregion volumes in violent or highly agitated schizophrenic patients compared to those with lower agitation, linking OFC morphology with emotional regulation and impulsivity, although findings are somewhat inconsistent across studies (Dong et al., 2025; Chen et al., 2022). These findings further support the hypothesis that OFC dysfunction contributes not only to negative affect and social withdrawal, but also to impulsivity and disinhibition frequently observed in SCZ. While most studies report reductions in networklevel measures among patients, there is a subset of the literature documenting selective increases under specific conditions, suggesting a more complex pattern of dysregulation (Zhang et al., 2022; Hadley et al., 2016; Sokunbi et al., 2014).

Given the prominence of symptoms such as auditory and visual hallucinations in SCZ, it is not unexpected that the corresponding sensory networks have received attention in the literature. Research on dynamic functional connectivity has reported altered temporal variability and changes in nodal centrality within both the auditory and visual networks in patients. These disruptions may underlie the emergence of positive symptoms, such as auditory verbal hallucinations, lending further support to the hypothesis that sensory network dysfunction plays a role in the pathophysiology of hallucinations (You et al., 2021). Furthermore, a frequent finding of rs-fMRI research that has contrasted SCZ subjects with HC is reduced auditory network FC (Joo et al., 2020; Li et al., 2019; Woodruff et al., 1997). Such alterations may reflect abnormal integration or insufficient inhibition within primary and secondary auditory cortices. Supporting this, a meta-analysis of ICA-based resting-state fMRI studies reported reduced functional connectivity in SCZ patients compared to healthy controls within both the AN and CON, highlighting their central roles in aberrant information processing (Li et al., 2019). Dysfunctions in early sensory processing may cascade into higher-order associative disturbances, potentially contributing to the emergence of hallucinations. This aligns with our findings, which point to dissociable network-level disruptions that may underlie specific clinical symptoms of SCZ - an interpretation further supported by existing literature. Alternatively, evidence validates that impaired connectivity among other large-scale brain networks, i.e., the SN and the DMN, can lead to compensatory hyperactivity of AN (Mallikarjun et al., 2018).

Our findings of disrupted connectivity across the CON, FPN, and DMN are consistent with prior research implicating such disruptions in the impaired cognitive control and sustained attention characteristic of SCZ (Repovs et al., 2011). Moreover, this study provides further validation for established research on CON hypoconnectivity in SCZ and the functional disconnections within cortico-striatal circuits of the CON, which have been linked to negative symptom severity (Tu et al., 2012). Conversely, the literature is not entirely consistent regarding these group-level differences. One particular study, for example, found no significant differences in CON and FPN connectivity when comparing SCZ patients with HC (Sheffield et al., 2015). These variations highlight the multidimensionality of large-scale network disruptions in SCZ, offering an explanation for divergent findings based on clinical characteristics, illness stages, or analytical methods.

EHN alterations observed in our study align with previous investigations of this region. Although fMRI studies targeting specifically the EHN in SCZ remain limited, structural MRI and histopathological studies report abnormalities in this region. Some studies have observed volume reduction and cytoarchitectural disturbance in the entorhinal cortex in patients with SCZ, particularly in antipsychotic-naive populations (Jose et al., 2012; Nasrallah et al., 1997; Arnold, 1991). These findings indicate that the entorhinal cortex, a key node for associative and memory processing, undergoes structural alterations even at the early stage of the disease. Furthermore, reduced resting-state modularity of the hippocampal-medial temporal lobe cortex network, which includes the entorhinal cortex, has been previously associated with relational memory impairment in patients (Avery et al., 2018). Additionally, decreased functional connectivity between hippocampuscircuits and subcortical circuits also supports the concept of disrupted EHN integration (Gangadin et al., 2021). These findings underscore the critical role of entorhinal-hippocampal dysconnectivity in the cognitive and large-scale network impairments observed in SCZ.

The DMN has been extensively investigated in SCZ, consistently revealing disruptions in its network organization and functional connectivity. Expanding on this, our results specifically showed a significant difference in DMN participation coefficient when comparing patients with HC. Notably, reduced DMN efficiency, particularly within its core

Table 8
Correlations between averaged Eigenvector Centrality (EC), Node Strength (NS), Clustering Coefficient (CC) in participation coefficient (PC) at the macro level across predefined large-scale networks (LSNs) and total PANSS score.

LSN	r EC	p	r NS	p	r CC	p	r PC	p
AN	0,1434	0,359	-0,009	0,9542	0,0169	0,9145	-0,0562	0,7206
CON	-0,1675	0,283	-0,2167	0,1629	-0,2148	0,1666	0,1535	0,3258
Context	-0,2119	0,1726	-0,3192	0,037*	-0,3118	0,0418*	-0,1324	0,3974
DMN	0,1526	0,3285	-0,1303	0,405	-0,077	0,6235	0,1215	0,4378
DAN	0,1496	0,3383	-0,076	0,6283	-0,051	0,7454	-0,0849	0,5883
perN	0,0034	0,9826	-0,0452	0,7734	-0,0341	0,8283	-0,2486	0,108
SMN	-0,1773	0,2554	-0,226	0,1451	-0,2231	0,1504	-0,0249	0,8739
Striatum	0,2045	0,1883	0,0586	0,7089	0,0792	0,6138	0,0083	0,958
Th	-0,1367	0,3819	-0,2274	0,1424	-0,2289	0,1398	0,0904	0,5643
VAN	0,0813	0,6041	-0,1801	0,2479	-0,1498	0,3376	0,1259	0,4212
Visual	-0,0336	0,8305	-0,1183	0,4498	-0,1162	0,458	-0,1249	0,4248
FPN	0,1093	0,4852	-0,0112	0,9429	0,0213	0,8922	0,0078	0,9606
SN	-0,1346	0,3895	-0,0846	0,5898	-0,0598	0,7031	-0,1453	0,3527
Amygdala	-0,0992	0,5268	-0,1197	0,4445	-0,1777	0,2542	0,0404	0,7971
EHN	-0,1014	0,5176	-0,0341	0,828	-0,0068	0,9655	-0,2038	0,19

^{*} indicates significant changes; no correlations survive the Benjamini-Hochberg correction.

Table 9
Correlations between averaged Eigenvector Centrality (EC), Node Strength (NS), Clustering Coefficient (CC) in participation coefficient (PC) at the macro level across predefined large-scale networks (LSNs) and PANSSP score.

LSN	r EC	p	r NS	p	r CC	p	r PC	p
AN	-0,017	0,914	-0,0479	0,7602	-0,0436	0,7812	-0,0522	0,7398
CON	-0,0004	0,9979	-0,1041	0,5065	-0,1165	0,4571	0,218	0,1601
Context	-0,2644	0,0866	-0,3181	0,0376*	-0,3258	0,033*	-0,0744	0,6355
DMN	0,1654	0,2891	-0,0068	0,9654	0,0302	0,8476	0,1773	0,2553
DAN	-0,0323	0,8371	-0,0485	0,7575	-0,0502	0,7493	0,0563	0,7197
perN	0,0338	0,8297	-0,0101	0,9489	-0,0222	0,8878	-0,1642	0,2928
SMN	0,0181	0,9081	-0,1181	0,4508	-0,1297	0,4072	0,1712	0,2722
Striatum	0,2665	0,0841	0,1548	0,3216	0,1549	0,3214	-0,2665	0,0841
Th	0,021	0,8936	-0,1167	0,4563	-0,1315	0,4006	0,2705	0,0794
VAN	0,2006	0,1971	-0,0706	0,6527	-0,0344	0,8264	0,0673	0,6683
Visual	-0,0535	0,7333	-0,1129	0,4711	-0,1339	0,3919	-0,0777	0,6203
FPN	0,2275	0,1424	0,022	0,8884	0,036	0,8188	0,0981	0,5315
SN	-0,0754	0,631	-0,0283	0,8569	-0,0194	0,902	-0,0019	0,9902
Amygdala	-0,1375	0,3792	-0,0719	0,6467	-0,1164	0,4574	-0,1641	0,2929
EHN	0,0193	0,902	0,037	0,8138	0,0457	0,771	-0,0712	0,6502

^{*} indicates significant changes; no correlations survive the Benjamini–Hochberg correction.

Table 10
Correlations between averaged Eigenvector Centrality (EC), Node Strength (NS), Clustering Coefficient (CC) in participation coefficient (PC) at the macro level across predefined large-scale networks (LSNs) and PANSSN score.

7.037	T.C		NO				D.C.	
LSN	r EC	p	r NS	p	r CC	p	r PC	p
AN	0,1489	0,3407	-0,0407	0,7957	-0,0059	0,9701	-0,0382	0,808
CON	-0,3336	0,0288*	-0,3273	0,0321*	-0,312	0,0417*	0,0953	0,5431
Context	-0,1827	0,241	-0,2512	0,1042	-0,2176	0,1611	-0,1692	0,2782
DMN	0,031	0,8433	-0,2833	0,0656	-0,2344	0,1302	0,039	0,8041
DAN	0,1354	0,3867	-0,1732	0,2667	-0,1316	0,4002	-0,1977	0,2038
perN	-0,0647	0,6802	-0,1553	0,3201	-0,1439	0,3573	-0,2753	0,074
SMN	-0,3518	0,0207*	-0,319	0,0371*	-0,3007	0,0501	-0,2736	0,0759
Striatum	-0,0128	0,9352	-0,1517	0,3315	-0,1235	0,4299	0,3001	0,0506
Th	-0,3268	0,0324*	-0,33	0,0307*	-0,3165	0,0387*	-0,1219	0,4361
VAN	-0,2143	0,1677	-0,3113	0,0421*	-0,2945	0,0552	0,1227	0,4333
Visual	0,0224	0,8866	-0,1637	0,2943	-0,1236	0,4298	-0,1847	0,2358
FPN	-0,1651	0,29	-0,1831	0,24	-0,1651	0,2902	-0,1323	0,3977
SN	-0,2098	0,1769	-0,2234	0,1498	-0,215	0,1661	-0,2717	0,078
Amygdala	-0,1051	0,5025	-0,2186	0,159	-0,2556	0,0981	0,1553	0,3201
EHN	-0,1824	0,2418	-0,2038	0,19	-0,182	0,2429	-0,3523	0,0205*

 $^{^{\}ast}$ indicates significant changes; no correlations survive the Benjamini–Hochberg correction.

medial temporal lobe subsystem, has been linked to negative symptoms like apathy and avolition (Cao et al., 2025). In addition, aberrant DMN activity has also been implicated in cognitive impairment, with cognitively impaired patients having been shown to have reduced suppression of the core DMN areas such as medial prefrontal cortex and posterior cingulate cortex during task performance (Zhou et al., 2016).

In this regard, our findings align with existing evidence suggesting disrupted DMN integration, which may be linked to negative symptoms. However, this view is not universally accepted. Some research indicates that DMN connectivity reductions are more closely associated with positive and affective symptoms than with negative symptoms, and that DMN abnormalities differ depending on cognitive status and

Table 11
Correlations between averaged Eigenvector Centrality (EC), Node Strength (NS), Clustering Coefficient (CC) in participation coefficient (PC) at the macro level across predefined large-scale networks (LSNs) and PANSSG score; there are no significant correlations.

LSN	r EC	p	r NS	p	r CC	p	r PC	p
PANSSG	r EC	p	r NS	p	r CC	p	r PC	p
AN	0,1741	0,2643	0,0372	0,8127	0,0593	0,7057	-0,0493	0,7536
CON	-0,0844	0,5903	-0,1222	0,4348	-0,1223	0,4345	0,099	0,5276
Context	-0,1224	0,4343	-0,2449	0,1135	-0,2497	0,1063	-0,0895	0,568
DMN	0,1699	0,2761	-0,046	0,7697	-0,0009	0,9954	0,1004	0,522
DAN	0,2031	0,1914	0,0032	0,9838	0,0223	0,8873	-0,0547	0,7275
perN	0,0313	0,842	0,0267	0,865	0,0463	0,768	-0,1832	0,2396
SMN	-0,1005	0,5212	-0,1374	0,3795	-0,138	0,3774	0,0439	0,78
Striatum	0,2395	0,1218	0,1252	0,4236	0,1442	0,3563	-0,0399	0,7994
Th	-0,0439	0,7797	-0,1334	0,3937	-0,1371	0,3805	0,1	0,5235
VAN	0,1841	0,2373	-0,0839	0,5928	-0,0593	0,7056	0,1129	0,4712
Visual	-0,0477	0,7612	-0,046	0,7695	-0,0575	0,7141	-0,0634	0,6861
FPN	0,1879	0,2275	0,0905	0,5637	0,1309	0,4029	0,0494	0,7529
SN	-0,0657	0,6757	0,01	0,949	0,0451	0,7738	-0,0842	0,5913
Amygdala	-0,0366	0,8159	-0,0341	0,8282	-0,0919	0,5579	0,0606	0,6995
EHN	-0,0752	0,6319	0,0539	0,7313	0,0849	0,5882	-0,0998	0,5243

clinical outcome (Lee et al., 2019). The heterogeneity suggests that SCZ's DMN dysfunction is multifaceted and symptom profiles and illness stages are likely to be responsible for these network alterations.

5. Limitations

While this study provides novel insights into hierarchical network disruptions in schizophrenia, several limitations should be acknowledged. First, all patients included in the study had severe auditory verbal hallucinations, which may limit the generalizability of our findings to schizophrenia patients without this symptom profile. Second, we performed formal statistical analyses to correlate network measures with clinical symptom severity (PANSS scores). There were significant results, but they did not survive correction for multiple comparisons, indicating they should be interpreted with caution and precluding definitive clinical inferences. One possible explanation for this finding is that FDR or Bonferroni corrections become overly conservative when applied to more than ten comparisons (in our case, fifteen). The same applies to comparing network measures between groups, which results in few significant effects after correction. Moreover, this finding reflects the limitations of clinical observer-based rating scales, as discussed elsewhere (Di Nicola and Stoyanov, 2021). Third, all patients were receiving stable doses of atypical antipsychotics at the time of scanning, and we did not control for potential medication effects on functional connectivity patterns. These pharmacological influences could have modulated the observed network alterations, though the direction and magnitude of such effects remain unclear. Future studies incorporating unmedicated patients and systematic symptom-network correlations would help address these limitations. Another limitation is the translation of the results into clinical reasoning.

6. Conclusions

This multi-level fMRI study advances our understanding of schizophrenia by demonstrating that the disorder arises from hierarchical disruptions in brain network organization. At the macroscale level, we identified a fundamental imbalance in integration-segregation dynamics, characterized by pathologically elevated participation coefficients in higher-order cognitive networks including the DMN and DAN. These macroscale disturbances co-occur with localized circuit failures, most prominently in temporal-orbitofrontal-cingulate pathways, creating a dual pathology where global hyperconnectivity masks critical local disconnections. The orbitofrontal cortex emerges as a pivotal hub in this system, with its structural deficits driving functional

disintegration that underlies negative and impulsive symptoms, while sensory network vulnerabilities may provide mechanistic explanations for hallucinatory phenomena.

The impact of this work advances the field in several dimensions. Methodologically, our multi-level framework is promising for resolving longstanding challenges in reconciling seemingly contradictory findings of both hyper- and hypoconnectivity in SCZ by demonstrating how these phenomena coexist at different hierarchical levels. Clinically, we identify distinct network biomarkers for core symptom domains: sensory network vulnerabilities correlate with hallucinations, orbitofrontal-thalamic disconnection underlies negative symptoms, and dorsal attention network alterations reflect compensatory mechanisms. These findings provide actionable targets for developing circuit-specific interventions. The multigraph model particularly demonstrates how reduced centrality of high-level cognitive networks and orbitofrontal-thalamic-amygdala circuits distinguishes patients from healthy controls. These network signatures offer new possibilities for precision medicine approaches.

Theoretically, the demonstrated hierarchy of disruptions – from dysfunction in local level to impaired global network integration – provides a testable framework that unites neurodevelopmental hypotheses with observed clinical manifestations. Our approach, which spans multiple network levels, explains previously paradoxical findings of coexisting hyper- and hypoconnectivity in schizophrenia. It also establishes a new paradigm for investigating complex neuropsychiatric disorders. Future research should focus on longitudinal tracking of network evolution during disease progression, targeted intervention trials, and translation of multigraph modeling into clinical stratification tools. These advances move the field toward biologically grounded subtyping of schizophrenia and personalized therapeutic strategies based on individual network profiles.

CRediT authorship contribution statement

V.S. Khorev: Writing – original draft, Visualization, Software, Methodology, Investigation, Conceptualization. S.A. Kurkin: Writing – original draft, Visualization, Software, Project administration, Methodology, Conceptualization. D. Stoyanov: Writing – review & editing, Validation, Supervision, Resources, Methodology, Investigation, Data curation, Conceptualization. R. Paunova: Writing – review & editing, Validation, Resources, Data curation, Conceptualization. D. Najar: Writing – review & editing, Validation, Investigation, Data curation. S. Kandilarova: Writing – review & editing, Methodology, Investigation, Data curation. A.E. Hramov: Writing – review & editing, Supervision, Resources, Project administration, Methodology, Investigation, Funding acquisition, Conceptualization.

Declaration of competing interest

The authors declare that they have no known competing financial interests or personal relationships that could have appeared to influence the work reported in this paper.

Appendix

See Tables 8-11.

Data availability

The data that support the findings of this study are not openly available due to reasons of sensitivity and are available from the corresponding author upon reasonable request.

References

- Andreev, A.V., Kurkin, S.A., Stoyanov, D., Badarin, A.A., Paunova, R., Hramov, A.E., 2023. Toward interpretability of machine learning methods for the classification of patients with major depressive disorder based on functional network measures. Chaos Interdiscip. J. Nonlinear Sci. 33 (6), 063140. http://dx.doi.org/10.1063/5.0155567.
- Arnold, s.E., 1991. Some cytoarchitectural abnormalities of the entorhinal cortex in schizophrenia. Arch. Gen. Psychiatry 48 (625), http://dx.doi.org/10.1001/archpsyc. 1991.01810310043008.
- Avery, S., Armstrong, K., Rogers, B., Heckers, S., 2018. T220. hippocampal network dysfunction and relational memory deficits in schizophrenia. Biol. Psychiatry 83, S213–S214. http://dx.doi.org/10.1016/j.biopsych.2018.02.557.
- Buckner, R.L., 2013. The brain's default network: origins and implications for the study of psychosis. Dialogues Clin. Neurosci. 15, 351–358. http://dx.doi.org/10.31887/ dcns.2013.15.3/rbuckner.
- Cao, C., Liu, W., Hou, C., Chen, Y., Liao, F., Long, H., Chen, D., Chen, X., Li, F., Huang, J., Zhou, X., Luo, D., Qu, H., Zhao, G., 2025. Disrupted default mode network connectivity and its role in negative symptoms of schizophrenia. Psychiatry Res. 348, 116489. http://dx.doi.org/10.1016/j.psychres.2025.116489.
- Chatterjee, I., Hilal, B., 2024. Investigating the association between symptoms and functional activity in brain regions in schizophrenia: A cross-sectional fmri-based neuroimaging study. Psychiatry Res.: Neuroimaging 344, 111870.
- Chen, C., Yao, J., Lv, Y., Zhao, X., Zhang, X., Lei, J., Li, Y., Sui, Y., 2022. Aberrant functional connectivity of the orbitofrontal cortex is associated with excited symptoms in first-episode drug-naïve patients with schizophrenia. Front. Psychiatry 13, http://dx.doi.org/10.3389/fpsyt.2022.922272.
- Costantini, G., Perugini, M., 2014. Generalization of clustering coefficients to signed correlation networks. PLoS One 9, e88669.
- Di Nicola, V., Stoyanov, D., 2021. Methods for clinical evaluation in psychiatry: quantitative vs. qualitative approaches. In: Psychiatry in Crisis: At the Crossroads of Social Sciences, the Humanities, and Neuroscience. Springer, pp. 17–29.
- Dong, Y., Tang, Y., Li, Y., Cao, P., Xu, G., Zhu, R., Li, R., Sui, Y., 2025. Role of peripheral cytokines and orbitofrontal cortex subregion structure in schizophrenia agitation. Sci. Rep. 15. http://dx.doi.org/10.1038/s41598-025-99033-5.
- Dong, D., Wang, Y., Chang, X., Luo, C., Yao, D., 2018. Dysfunction of large-scale brain networks in schizophrenia: a meta-analysis of resting-state functional connectivity. Schizophr. Bull. 44, 168–181.
- Epstein, R.A., 2008. Parahippocampal and retrosplenial contributions to human spatial navigation. Trends Cogn. Sci. 12, 388–396.
- Friston, K., Brown, H.R., Siemerkus, J., Stephan, K.E., 2016. The dysconnection hypothesis (2016). Schizophr. Res. 176, 83–94. http://dx.doi.org/10.1016/j.schres. 2016.07.014.
- Gangadin, S.S., Cahn, W., Scheewe, T.W., Hulshoff Pol, H.E., Bossong, M.G., 2021. Reduced resting state functional connectivity in the hippocampus-midbrain-striatum network of schizophrenia patients. J. Psychiatr. Res. 138, 83–88. http://dx.doi.org/ 10.1016/j.jpsychires.2021.03.041.
- Guimera, R., Nunes Amaral, L.A., 2005. Functional cartography of complex metabolic networks. Nature 433, 895–900.
- Hadley, J.A., Kraguljac, N.V., White, D.M., Hoef, L.Ver., Tabora, J., Lahti, A.C., 2016. Change in brain network topology as a function of treatment response in schizophrenia: a longitudinal resting-state fmri study using graph theory. Npj Schizophr. 2, http://dx.doi.org/10.1038/npjschz.2016.14.
- Hardikar, S., Mckeown, B., Schaare, H.L., Wallace, R.S., Xu, T., Lauckener, M.E., Valk, S.L., Margulies, D.S., Turnbull, A., Bernhardt, B.C., et al., 2024. Macro-scale patterns in functional connectivity associated with ongoing thought patterns and dispositional traits. Elife 13, RP93689.
- Huang, H., Chen, C., Rong, B., Wan, Q., Chen, J., Liu, Z., Zhou, Y., Wang, G., Wang, H., 2022. Resting-state functional connectivity of salience network in schizophrenia and depression. Sci. Rep. 12. http://dx.doi.org/10.1038/s41598-022-15489-9.

- Isomura, S., Hashimoto, R., Nakamura, M., Hirano, Y., Yamashita, F., Jimbo, S., Yamamori, H., Fujimoto, M., Yasuda, Y., Mears, R.P., Onitsuka, T., 2017. Altered sulcogyral patterns of orbitofrontal cortex in a large cohort of patients with schizophrenia. Npj Schizophr. 3, http://dx.doi.org/10.1038/s41537-016-0008-y.
- Joo, S.W., Yoon, W., Jo, Y.T., Kim, H., Kim, Y., Lee, J., 2020. Aberrant executive control and auditory networks in recent-onset schizophrenia. Neuropsychiatr. Dis. Treat. 16, 1561–1570. http://dx.doi.org/10.2147/ndt.s254208.
- Jose, S.P., Sharma, E., Narayanaswamy, J.C., Rajendran, V., Kalmady, S.V., Rao, N.P., Venkatasubramanian, G., Gangadhar, B.N., 2012. Entorhinal cortex volume in antipsychotic-naäve schizophrenia. Indian J. Psychol. Med. 34, 164–169. http: //dx.doi.org/10.4103/0253-7176.101787.
- Kay, S.R., Fiszbein, A., Opler, L.A., 1987. The positive and negative syndrome scale (panss) for schizophrenia. Schizophr. Bull. 13, 261–276.
- Kelly, C., Castellanos, F.X., 2014. Strengthening connections: functional connectivity and brain plasticity. Neuropsychol. Rev. 24, 63–76.
- Khorev, V., Kurkin, S., Pitsik, E., Radutnaya, M., Bondar, E., Mayorova, L., Hramov, A., 2025. A synergistic approach for identifying disrupted functional brain subnetworks in patients with chronic disorders of consciousness due to anoxic brain damage. Eur. Phys. J. Spec. Top. 234, 4907–4918. http://dx.doi.org/10.1140/epjs/s11734-024-01454-2.
- Khorev, V.S., Kurkin, S.A., Zlateva, G., Paunova, R., Kandilarova, S., Maes, M., Stoyanov, D., Hramov, A.E., 2024. Disruptions in segregation mechanisms in fmribased brain functional network predict the major depressive disorder condition. Chaos Solitons Fractals 188, 115566.
- Kurkin, S., Mayorova, L., Khorev, V., Pitsik, E., Radutnaya, M., Bondar, E., Hramov, A., 2025. Multiscale fmri analysis reveals hierarchical network disruptions underlying disorders of consciousness. Chaos Solitons Fractals 200, 117008. http://dx.doi.org/ 10.1016/j.chaos.2025.117008.
- Kurkin, S.A., Smirnov, N.M., Paunova, R., Kandilarova, S., Stoyanov, D., Mayorova, L., Hramov, A.E., 2024. Beyond pairwise interactions: Higher-order q-analysis of fmribased brain functional networks in patients with major depressive disorder. IEEE Access 12, 197168–197186. http://dx.doi.org/10.1109/ACCESS.2024.3521249.
- Lee, J.S., Chun, J.W., Lee, S.H., Kim, E., Lee, S.K., Kim, J.J., 2015. Altered neural basis of the reality processing and its relation to cognitive insight in schizophrenia. PLoS One 10, e0120478.
- Lee, H., Lee, D.K., Park, K., Kim, C.E., Ryu, S., 2019. Default mode network connectivity is associated with long-term clinical outcome in patients with schizophrenia. NeuroImage: Clin. 22, 101805. http://dx.doi.org/10.1016/j.nicl.2019.101805.
- Li, S., Hu, N., Zhang, W., Tao, B., Dai, J., Gong, Y., Tan, Y., Cai, D., Lui, S., 2019. Dysconnectivity of multiple brain networks in schizophrenia: A meta-analysis of resting-state functional connectivity. Front. Psychiatry 10. http://dx.doi.org/10.3389/fpsyt.2019.00482.
- Liang, S., Wang, Q., Greenshaw, A.J., Li, X., Deng, W., Ren, H., Zhang, C., Yu, H., Wei, W., Zhang, Y., Li, M., Zhao, L., Du, X., Meng, Y., Ma, X., Yan, C.G., Li, T., 2021. Aberrant triple-network connectivity patterns discriminate biotypes of first-episode medication-naive schizophrenia in two large independent cohorts. Neuropsychopharmacology 46, 1502–1509. http://dx.doi.org/10.1038/s41386-020-00926-y.
- Lynall, M.E., Bassett, D.S., Kerwin, R., McKenna, P.J., Kitzbichler, M., Muller, U., Bullmore, E., 2010. Functional connectivity and brain networks in schizophrenia. J. Neurosci. 30, 9477–9487. http://dx.doi.org/10.1523/jneurosci.0333-10.2010.
- Mallikarjun, P.K., Lalousis, P.A., Dunne, T.F., Heinze, K., Reniers, R.L., Broome, M.R., Farmah, B., Oyebode, F., Wood, S.J., Upthegrove, R., 2018. Aberrant salience network functional connectivity in auditory verbal hallucinations: a first episode psychosis sample. Transl. Psychiatry 8, http://dx.doi.org/10.1038/s41398-018-0118-6.
- Menon, V., 2023. 20 years of the default mode network: A review and synthesis. Neuron 111, 2469–2487. http://dx.doi.org/10.1016/j.neuron.2023.04.023.
- Nakamura, M., Nestor, P.G., Levitt, J.J., Cohen, A.S., Kawashima, T., Shenton, M.E., McCarley, R.W., 2007. Orbitofrontal volume deficit in schizophrenia and thought disorder. Brain 131, 180–195. http://dx.doi.org/10.1093/brain/awm265.
- Nasrallah, H.A., Sharma, S., Olson, S.C., 1997. The volume of the entorhinal cortex in schizophrenia: A controlled mri study. Prog. Neuropsychopharmacol. Biol. Psychiatry 21, 1317–1322. http://dx.doi.org/10.1016/s0278-5846(97)00166-8.
- Newman, M.E., 2008. The mathematics of networks. New Palgrave Encycl. Econ. 2, 1-12.
- Núñez, C., Stephan-Otto, C., Roldán, A., Grasa, E.M., Escartí, M.J., Aguilar García-Iturrospe, E.J., García-Martí, G., de la Iglesia-Vaya, M., Nacher, J., Portella, M.J., Corripio, I., 2024. Orbitofrontal cortex hypergyrification in hallucinating schizophrenia patients: Surface ratio as a promising brain biomarker. Eur. Neuropsychopharmacol. 89, 47–55. http://dx.doi.org/10.1016/j.euroneuro.2024.
- Onnela, J.P., Saramäki, J., Kertész, J., Kaski, K., 2005. Intensity and coherence of motifs in weighted complex networks. Phys. Rev. E—Statistical, Nonlinear, Soft Matter Phys. 71, 065103.

- Pisarchik, A.N., Andreev, A.V., Kurkin, S.A., Stoyanov, D., Badarin, A.A., Paunova, R., Hramov, A.E., 2023. Topology switching during window thresholding fmri-based functional networks of patients with major depressive disorder: Consensus network approach. Chaos: An Interdiscip. J. Nonlinear Sci. 33 (9), 093122. http://dx.doi. org/10.1063/5.0166148.
- Pitsik, E.N., Maximenko, V.A., Kurkin, S.A., Sergeev, A.P., Stoyanov, D., Paunova, R., Kandilarova, S., Simeonova, D., Hramov, A.E., 2023. The topology of fmri-based networks defines the performance of a graph neural network for the classification of patients with major depressive disorder. Chaos Solitons Fractals 167, 113041.
- Repovs, G., Csernansky, J.G., Barch, D.M., 2011. Brain network connectivity in individuals with schizophrenia and their siblings. Biol. Psychiatry 69, 967–973. http://dx.doi.org/10.1016/j.biopsych.2010.11.009.
- Rolls, E.T., Huang, C.C., Lin, C.P., Feng, J., Joliot, M., 2020. Automated anatomical labelling atlas 3. Neuroimage 206, 116189.
- Rubinov, M., Sporns, O., 2011. Weight-conserving characterization of complex functional brain networks. Neuroimage 56, 2068–2079.
- Sheehan, D.V., Lecrubier, Y., Sheehan, K.H., Amorim, P., Janavs, J., Weiller, E., Hergueta, T., Baker, R., Dunbar, G.C., et al., 1998. The mini-international neuropsychiatric interview (mini): the development and validation of a structured diagnostic psychiatric interview for dsm-iv and icd-10. J. Clin. Psychiatry 59, 22–33.
- Sheffield, J.M., Repovs, G., Harms, M.P., Carter, C.S., Gold, J.M., MacDonald III, A.W., Ragland, J.Daniel., Silverstein, S.M., Godwin, D., Barch, D.M., 2015. Fronto-parietal and cingulo-opercular network integrity and cognition in health and schizophrenia. Neuropsychologia 73, 82–93. http://dx.doi.org/10.1016/j.neuropsychologia.2015. 05.006.
- Skåtun, K.C., Kaufmann, T., Tønnesen, S., Biele, G., Melle, I., Agartz, I., Alnæs, D., Andreassen, O.A., Westlye, L.T., 2016. Global brain connectivity alterations in patients with schizophrenia and bipolar spectrum disorders. J. Psychiatry Neurosci. 41, 331–341. http://dx.doi.org/10.1503/jpn.150159.
- Sokunbi, M.O., Gradin, V.B., Waiter, G.D., Cameron, G.G., Ahearn, T.S., Murray, A.D., Steele, D.J., Staff, R.T., 2014. Nonlinear complexity analysis of brain fmri signals in schizophrenia. PLoS ONE 9, e95146. http://dx.doi.org/10.1371/journal.pone. 0095146.
- SPM, 2024. Spm12. http://www.fil.ion.ucl.ac.uk/spm. (Accessed 12 April 2024).
- Stoyanov, D., Kandilarova, S., Aryutova, K., Paunova, R., Todeva-Radneva, A., Laty-pova, A., Kherif, F., 2020. Multivariate analysis of structural and functional neuroimaging can inform psychiatric differential diagnosis. Diagnostics 11 (19).
- Tu, P.C., Hsieh, J.C., Li, C.T., Bai, Y.M., Su, T.P., 2012. Cortico-striatal disconnection within the cingulo-opercular network in schizophrenia revealed by intrinsic functional connectivity analysis: A resting fmri study. NeuroImage 59, 238–247. http://dx.doi.org/10.1016/j.neuroimage.2011.07.086.
- Uddin, L.Q., 2014. Salience processing and insular cortical function and dysfunction. Nature Rev. Neurosci. 16, 55–61, http://dx.doi.org/10.1038/nrn3857.
- Varaprasad, S., Goel, T., 2025. Exploring the significance of the frontal lobe for diagnosis of schizophrenia using explainable artificial intelligence and group level analysis. Psychiatry Res.: Neuroimaging 349, 111969.
- Voineskos, A.N., Hawco, C., Neufeld, N.H., Turner, J.A., Ameis, S.H., Anticevic, A., Buchanan, R.W., Cadenhead, K., Dazzan, P., Dickie, E.W., Gallucci, J., Lahti, A.C., Malhotra, A.K., Öngür, D., Lencz, T., Sarpal, D.K., Oliver, L.D., 2024. Functional magnetic resonance imaging in schizophrenia: current evidence, methodological advances, limitations and future directions. World Psychiatry 23, 26–51. http://dx.doi.org/10.1002/wps.21159.

- Walton, E., Hibar, D.P., van Erp, T.G.M., Potkin, S.G., Roiz-Santiañez, R., Crespo-Facorro, B., Suarez-Pinilla, P., van Haren, N.E.M., de Zwarte, S.M.C., Kahn, R.S., Cahn, W., Doan, N.T., Jørgensen, K.N., Gurholt, T.P., Agartz, I., Andreassen, O.A., Westlye, L.T., Melle, I., Berg, A.O., Morch-Johnsen, L., rden, A.Fæ., Flyckt, L., Fatouros-Bergman, H., Jönsson, E.G., Hashimoto, R., Yamamori, H., Fukunaga, M., Jahanshad, N., Rossi, P.De., Piras, F., Banaj, N., Spalletta, G., Gur, R.E., Gur, R.C., Wolf, D.H., Satterthwaite, T.D., Beard, L.M., Sommer, I.E., Koops, S., Gruber, O., Richter, A., Krämer, B., Kelly, S., Donohoe, G., McDonald, C., Cannon, D.M., Corvin, A., Gill, M., Giorgio, A.Di., Bertolino, A., Lawrie, S., Nickson, T., Whalley, H.C., Neilson, E., Calhoun, V.D., Thompson, P.M., Turner, J.A., Ehrlich, S., 2017. Prefrontal cortical thinning links to negative symptoms in schizophrenia via the enigma consortium. Psychol. Med. 48, 82–94. http://dx.doi.org/10.1017/s0033291717001283.
- Wang, C., Cai, H., Sun, X., Si, L., Zhang, M., Xu, Y., Qian, Y., Zhu, J., 2020. Large-scale internetwork functional connectivity mediates the relationship between serum triglyceride and working memory in young adulthood. Neural Plast. 2020, 8894868.
- Whitfield-Gabrieli, S., Ford, J.M., 2012. Default mode network activity and connectivity in psychopathology. Annu. Rev. Clin. Psychol. 8, 49–76.
- Więcławski W. Bielski, K., Jani, M., Binder, M., Adamczyk, P., 2024. Dysconnectivity of the cerebellum and somatomotor network correlates with the severity of alogia in chronic schizophrenia. Psychiatry Res.: Neuroimaging 345, 111883.
- Woodruff, P.W., Wright, I.C., Bullmore, E.T., Brammer, M., Howard, R.J., Williams, S.C., Shapleske, J., Rossell, S., David, A.S., McGuire, P.K., Murray, R.M., 1997. Auditory hallucinations and the temporal cortical response to speech in schizophrenia: A functional magnetic resonance imaging study. Am. J. Psychiatry 154, 1676–1682. http://dx.doi.org/10.1176/ajp.154.12.1676.
- Yang, S.Q., Xu, Z.P., Xiong, Y., Zhan, Y.F., Guo, L.Y., Zhang, S., Jiang, R.F., Yao, Y.H., Qin, Y.Y., Wang, J.Z., et al., 2016. Altered intranetwork and internetwork functional connectivity in type 2 diabetes mellitus with and without cognitive impairment. Sci. Rep. 6 (32980).
- You, W., Luo, L., Li, F., Gong, Q., 2021. Altered brain functional dynamics in auditory and visual networks in schizophrenia. Eur. Psychiatry 64, http://dx.doi.org/10. 1192/j.eurpsy.2021.428, S159-S159.
- Zalesky, A., Fornito, A., Bullmore, E.T., 2010. Network-based statistic: identifying differences in brain networks. Neuroimage 53, 1197–1207.
- Zaykova, V., Kandilarova, S., Paunova, R., Ahmed-Popova, F., Stoyanov, D., 2025.
 Lateralized brain connectivity in auditory verbal hallucinations: fmri insights into the superior and middle temporal gyri, Front. Hum. Neurosci. 19, 1650178.
- Zhang, G., Cai, B., Zhang, A., Tu, Z., Xiao, L., Stephen, J.M., Wilson, T.W., Calhoun, V.D., Wang, Y.P., 2022. Detecting abnormal connectivity in schizophrenia via a joint directed acyclic graph estimation model. NeuroImage 260, 119451. http://dx.doi.org/10.1016/j.neuroimage.2022.119451.
- Zhang, L., Wang, W., Ruan, Y., Li, Z., Ji, G.J., Tian, Y., Wang, K., et al., 2024. Hyperactivity and altered functional connectivity of the ventral striatum in schizophrenia compared with bipolar disorder: A resting state fmri study. Psychiatry Res.: Neuroimaging 345, 111881.
- Zhou, L., Pu, W., Wang, J., Liu, H., Wu, G., Liu, C., Mwansisya, T.E., Tao, H., Chen, X., Huang, X., Lv, D., Xue, Z., Shan, B., Liu, Z., 2016. Inefficient dmn suppression in schizophrenia patients with impaired cognitive function but not patients with preserved cognitive function. Sci. Rep. 6. http://dx.doi.org/10.1038/srep21657.
- Zwir, I., Arnedo, J., Mesa, A., Val, C.Del., de Erausquin, G.A., Cloninger, C.R., 2023. Temperament & character account for brain functional connectivity at rest: A diathesis-stress model of functional dysregulation in psychosis. Mol. Psychiatry 28, 2238–2253.